RSC Advances

PAPER

View Article Online
View Journal | View Issue

Cite this: *RSC Adv.*, 2025, **15**, 47148

Smart controlled-release delivery of *Pennisetum purpureum* embedded supramolecular nanoparticles to reduce atherosclerotic plaque

Fasih Bintang Ilhami, *[a] Mufidatul Khasanah,[a] Wahyu Satriyo Wibowo,[a] Sapti Puspitarini,[a] Sari Edi Cahyaningrum, [b] Jindrayani Nyoo Putro,[cd] Astrid Rahmawati[e] and Huynh-Quang-Dieu Nguyen[f]

Vascular disease continues to be the primary cause of mortality and disability, often attributed to atherosclerosis. The present pharmacological treatment of atherosclerosis has limited therapeutic effectiveness. Herein, we report the synthesis of supramolecular nanoparticles through host–guest interactions involving β-cyclodextrin (β-CD), polypropylene glycol (PPG), and folic acid (FA) to create FA-PPG-β-CD, which effectively encapsulates bioactive compounds from *Pennisetum purpureum* extract for the smart control release of foam cells in atherosclerotic plaques. *Pennisetum purpureum*-loaded nanoparticles can spontaneously self-assemble into nanostructures, exhibiting unique characteristics such as intrinsic green fluorescence and high structural stability. More importantly, nanoparticles embedded with *Pennisetum purpureum* exhibit well-controlled drug release due to their thermoresponsive properties. Moreover, an *in vitro* investigation revealed that *Pennisetum purpureum*-loaded nanoparticles reduced foam cell production due to the elevated temperature associated with inflammatory conditions. Notably, *in vivo* studies have shown that *Pennisetum purpureum*-loaded nanoparticles rapidly eliminate excess foam cells from atherogenic lesions in the abdominal aorta. Moreover, *in vivo* hematology, liver, and kidney function values remained within physiological limits following treatment with *Pennisetum purpureum*-loaded nanoparticles, indicating excellent biocompatibility and no adverse effects on other organs. To the best of our knowledge, this is the first report of supramolecular nanoparticles encapsulating bioactive compounds from *Pennisetum purpureum* extract for targeting foam cells in inflammatory diseases.

Received 3rd October 2025
Accepted 24th November 2025

DOI: 10.1039/d5ra07519j

rsc.li/rsc-advances

Introduction

Cardiovascular disease (CVD) remains the foremost cause of death across all populations, primarily due to its association with atherosclerosis, a condition characterized by the buildup of plaque in arterial walls.[1–3] Although the pathogenesis of atherosclerosis is not yet fully understood, it is commonly initiated by endothelial dysfunction, which promotes the accumulation of oxidized low-density lipoprotein (oxLDL) within the intimal layer, leading to the activation of localized inflammation and excessive production of reactive oxygen species (ROS).[4,5] Inflammatory sites recruit circulating monocytes, which differentiate into macrophages. Upon internalizing oxLDL, these macrophages may undergo cell death or rupture, thereby intensifying the local inflammatory response through a positive feedback mechanism that promotes further recruitment of immune cells to the affected area.[6,7] Due to the vascular inflammation in endothelium cells, monocytes in the blood vessels penetrate the tunica intima and develop into macrophages.[8] The macrophages absorb a large amount of oxLDL and provide apolipoprotein B peptides to T cells, promoting cytokine generation.[9] When macrophages undergo excessive phagocytosis of oxLDL *via* scavenger receptors, they form foam cells that release interleukin-1β (IL-1β) cytokines, triggering inflammation during the early stages and progression of atherosclerosis.[10] Moreover, inflammation during atherosclerosis development may lead to significant temperature increase beyond normal body temperature (36.5–37.5 °C), characterized by thin fibrous caps, pronounced inflammatory activity, and

[a]*Department of Natural Science Faculty of Mathematics and Natural Science, Universitas Negeri Surabaya, Surabaya 60231, Indonesia. E-mail: fasihilhami@unesa.ac.id; saptipuspitarini@unesa.ac.id*

[b]*Department of Chemistry, Faculty of Mathematics and Natural Sciences, Universitas Negeri Surabaya, Surabaya 60231, Indonesia*

[c]*Chemical Engineering Master Program, Faculty of Engineering, Widya Mandala Surabaya Catholic University, Kalijudan 37, Surabaya 60114, Indonesia*

[d]*Collaborative Research Center for Sustainable and Zero Waste Industries, Jl. Kalijudan 37, Surabaya 60114, East Java, Indonesia*

[e]*Department of Applied Chemistry, Osaka Institute of Technology, Osaka 535-8585, Japan*

[f]*University of Colorado Denver, Anschutz Medical Campus, 2115 N Scranton Street, Aurora, CO 80045, USA*

surrounding lipid-rich cores.[11,12] The foam cells play a pivotal role in cholesterol deposition, and the development of atherosclerotic plaques leads to cell rupture and resulting in CVD.[13] Notably, over the past decade, several studies have demonstrated that folic acid (FA) functions as a receptor and facilitates the delayed development of atherosclerosis in low-density lipoprotein receptor-deficient ($LDLR^{-/-}$) mice, primarily due to its anti-apoptotic and antioxidative properties.[14,15] The targeted overexpression of folate receptors-β (FR-β) by activated macrophages, in contrast to resting macrophages or other immune cells, offers a significant possibility for the detection and treatment of inflammatory disorders, especially atherosclerosis.[16] For instance, Carnier and his co-worker[17] demonstrated in apolipoprotein E-deficient ($ApoE^{-/-}$) mice that the injection of FA led to a reduction in atherosclerotic lesions, correlated with elevated levels of apolipoproteins AI, AIV, and B, with a decrease in oxidative stress. Therefore, it is essential to develop an innovative and efficient strategy that incorporates folic acid and thermos-responsive properties to mitigate inflammation and the growth of foam cells in atherosclerosis.

The development of nanocarriers as a drug delivery system has attracted considerable interest in modern pharmaceutical technology due to their ability to improve therapeutic effectiveness and enable tailored intracellular administration for particular disorders. Supramolecular polymers are a category of polymers constructed from low-molecular-weight monomers by reversible non-covalent interactions.[18–20] Supramolecular polymeric nanoparticles (SPNs) have gained significant interest and emerged as an effective strategy for biomedical applications, owing to the dynamic and reversible characteristics of supramolecular chemistry, which bestow the resultant materials with exceptional stimuli-responsiveness and limitless potential.[21,22] In addition, the rapid structural disassembly of SPNs and well-controlled release of drugs in response to changes in their surrounding environment, which is influenced by a variety of stimuli, including pH,[23] temperature,[24] redox,[25] glucose,[26] light,[27] enzymes,[28,29] and other stimuli,[30–32] making them highly promising as drug delivery systems. More importantly, SPNs possessed significant enhancement of the solubility and stability of drugs through the formation of host–guest complexes or supramolecular assemblies.[33] Secondly, various functional groups, including target units, fluorescent moieties, and pro-drugs, may be readily incorporated into systems *via* dynamic and reversible supramolecular interactions.[34] Thirdly, due to the environmental disparities between normal and tumor tissues, the release of encapsulated drug molecules may be accurately controlled.[35] Macrocyclic compounds, including cyclodextrins, calixarenes, and pillararenes, serve as optimal platforms for the development of drug delivery system *via* supramolecular interactions, since they include size-controllable holes that allow for guest penetration.[36] Notwithstanding their numerous benefits, the advancement of supramolecular systems as therapeutic agents for vascular diseases such as atherosclerosis remains constrained, despite their considerable potential for these applications.

Numerous studies have shown that encapsulating bioactive compounds within nanoparticles can protect them from degradation, enhance their solubility and bioavailability, thereby enhancing their potential for biomedical applications.[37,38] Recently, Zhang and his colleagues[39] demonstrated that an extract from *Trifolium repens* leaves loaded into iron nanoparticles effectively protected the vessel wall from early atherosclerotic changes. However, these green formulations are limited by their poor solubility in blood, which might be due to the fact that they vary in the chemical nature of the compounds, which often restricts the incorporation of natural bioactive compound extracts into certain nanoparticle systems. More importantly, the controlled release of the extract from the nanoparticles is limited, making it difficult for the bioactive compound to effectively reach its target and act against early atherosclerotic alterations. Therefore, the development of nanoparticles with unique properties that can effectively encapsulate bioactive compounds and ensure their functional delivery are necessary.

Pennisetum purpureum, generally referred to as elephant grass, belongs to the Gramineae family and is widely used as cattle feed.[40,41] Due to the presence of polyphenolic chemicals in elephant grass, such as flavanols, catechins, and anthocyanins, elephant grass has been extensively used to regulate inflammation and immunological response.[41–43] Previously, our teams have explored the phytochemicals of *Pennisetum purpureum*, which include alkaloids, glycosides, saponins, steroids, and terpenoids. The qualitative analysis indicates that *Pennisetum purpureum* leaf extracts contain the highest levels of alkaloids and saponins. Both saponins and alkaloids exhibit analgesic, antibacterial, antihypertensive, and anti-inflammatory properties, whereas steroids primarily function as antibacterial agents. Notably, saponins are compounds that have rapid destruction of lipids in hyperlipidemia and act as antioxidants.[44–47] The chemical structure of saponins contains sugar groups linked to a triterpene or steroid aglycone, particularly glucose, galactose, xylose, rhamnose, or methyl pentose.[48] Hence, the bioactive compounds in *Pennisetum purpureum* are key factors that help reduce lipid levels and stabilize foam cells in blood vessels associated with atherosclerotic diseases.

In our previous study, we successfully synthesized a series of SPNs through host–guest interactions involving β-cyclodextrin (β-CD), polypropylene glycol (PPG), and folic acid (FA) to create FA-PPG-β-CD supramolecular nanoparticles encapsulating anticancer drugs.[49] These carriers spontaneously self-assemble into nanosized and comparatively stable nanostructures in an aqueous solution. Remarkably, anticancer drugs released by FA-PPG-β-CD supramolecular nanoparticles may be accurately modulated by adjusting the temperature, making them suitable for controlled drug delivery applications. To further extend the concept of supramolecular nanoparticles (SPNs) *via* host–guest interactions with bioactive compounds, we propose the design of smart controlled-release through host–guest interactions involving β-cyclodextrin (β-CD), polypropylene glycol (PPG), and folic acid (FA) to create FA-PPG-β-CD SPNs embedded with *Pennisetum purpureum* that can self-assemble into spherical nanostructures, producing high structural stability for the effective reduction and growth of foam cells in atherosclerotic plaques through thermoresponsiveness (Scheme 1). These

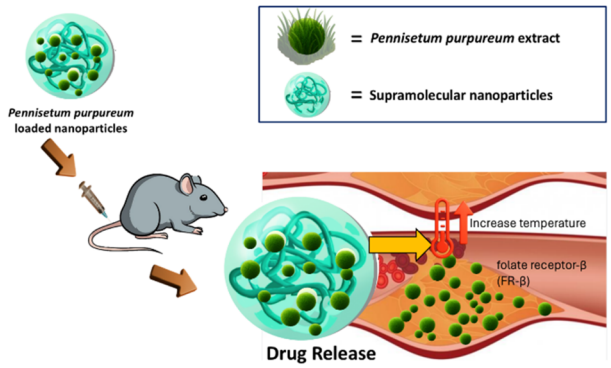

Scheme 1 Graphical representation of encapsulation of *Pennisetum purpureum* into supramolecular nanoparticles and as smart controlled release by thermos-responsive and folic acid for effective reduction of atherosclerotic plaque.

Pennisetum purpureum-embedded SPNs showed unique green fluorescence characteristics and well-controlled drug release of *Pennisetum purpureum* through thermosresponsive properties. More importantly, *in vitro* analysis clearly demonstrated that *Pennisetum purpureum*-loaded nanoparticles reduce inflammatory responses by being internalized into foam cell formation, due to the presence of FA and the release of bioactive compounds from *Pennisetum purpureum*. Computational simulations, including molecular docking and dynamic interaction analysis, provided insights into the molecular-level interaction mechanisms between FA-PPG-β-CD supramolecular nanoparticles and specific proteins in foam cells, exhibiting stable interaction behavior over time. Notably, *in vivo* studies demonstrated that *Pennisetum purpureum*-loaded SPNs rapidly destroy extra lipid in the aorta and abdominal aorta. To date, this is the first report of supramolecular nanoparticles encapsulating bioactive compounds from *Pennisetum purpureum* extract for targeting foam cells in inflammatory diseases. Thus, this novel *Pennisetum purpureum*-loaded nanoparticle system, developed by green synthesis, may serve as a multifunctional nanomaterial to mitigate inflammation and foam cell proliferation in atherosclerosis. Notably, these supramolecular nanoparticles would enhance the value and therapeutic potential of natural bioactive compounds, offering a safe and effective treatment approach for future biomedical applications.

Results and discussion

Our strategy focuses on multifunctional bioactive chemicals from *Pennisetum purpureum* extract, embedded into supramolecular nanoparticles (SPNs) from β-cyclodextrin (β-CD), polypropylene glycol (PPG), and folic acid (FA) forming FA-PPG-β-CD nanoparticles through inclusion complexes formed by host–guest interactions, which may be utilized as smart controlled-release reducing and growing by targeting foam cells in inflammatory diseases foam cells in atherosclerotic plaques through thermoresponsiveness (Scheme 1). Multifunctional FA-PPG-β-CD supramolecular nanoparticles through host–guest interaction were effectively synthesized using our previously outlined three-step reaction methods.[49] The extraction procedure of *Pennisetum purpureum*, which is centered on the qualitative and quantitative analysis of its phytochemical constituents, has been detailed in previous studies.[42] The extract yield of *Pennisetum purpureum* demonstrates phytochemical yield using ethanol solvent, revealing that alkaloids, flavonoids, saponins, and terpenoids are the predominant phytochemical compounds. More importantly, saponins are compounds that have been shown to rapidly destroy lipids in hyperlipidemia and act as antioxidants.[45–47] Due to substantial disparity in water solubility between *Pennisetum purpureum* leaf extract and supramolecular nanoparticles has prompted us to investigate *Pennisetum purpureum*-loaded nanoparticles in aqueous environments for the reduction of atherosclerotic plaque. We initially established self-assembled nanostructures of FA-PPG-β-CD supramolecular nanoparticles in an aqueous solution to facilitate the construction of drug encapsulation, as observed by DLS and SEM. As illustrated in Fig. S1a, the mean hydrodynamic particle sizes of FA-PPG-β-CD supramolecular nanoparticles were 86 nm, indicating that the polymer structure contained host–guest interactions that enabled self-assembly into nanosized particles in water. The DLS results were validated by SEM images, which confirmed that supramolecular nanoparticles formed spherical nanoparticles with a diameter of 40–55 nm (Fig. S1b). In contrast, pristine *Pennisetum purpureum* leaf extract had a mean hydrodynamic particle size of 3610 nm with a nonuniform and irregular structure (Fig. S2a and b).[54,55]

To further investigate our understanding of the self-assembled nanostructures formed by embedding *Pennisetum purpureum* into supramolecular nanoparticles, we evaluated them by directly mixing at various ratios using the dialysis method (Table S1). Interestingly, the highest integrated weight ratio of 2 : 1 indicated that the high payload content of *Pennisetum purpureum* within supramolecular nanoparticles achieved 18.03–1.89%, suggesting that host–guest interactions within the polymer augmented the affinity and specificity of the nanoparticles for *Pennisetum purpureum*, attribute to π–π stacking interactions between the hydrophobic *Pennisetum purpureum* and supramolecular nanoparticles, thereby a high drug loading capacity and stable drug entrapment was achieved.[56–58] Moreover, *Pennisetum purpureum*-loaded nanoparticles had an average particle diameter of 189 nm, indicating that the particle size of the nanoparticles increased to provide sufficient capacity for substantial drug payloads, compared to the pristine nanoparticles (Fig. 1a). In order to confirm these observations, SEM was implemented to observe the morphological structure of *Pennisetum purpureum*-loaded nanoparticles. As displayed in Fig. 1b, *Pennisetum purpureum*-loaded nanoparticles exhibit a smooth, spherical shape, with particle sizes ranging from 120 to 155 nm, which aligns with the DLS findings.

The optical characteristics of *Pennisetum purpureum*-loaded nanoparticles were analyzed using a UV-Vis spectrophotometer and photoluminescence (PL) spectroscopy. As shown in Fig. 1c, the distinctive absorption of *Pennisetum purpureum* extract occurs in the UV region with a mild peak absorption at a wavelength of 405 nm. Interestingly, *Pennisetum purpureum*-loaded

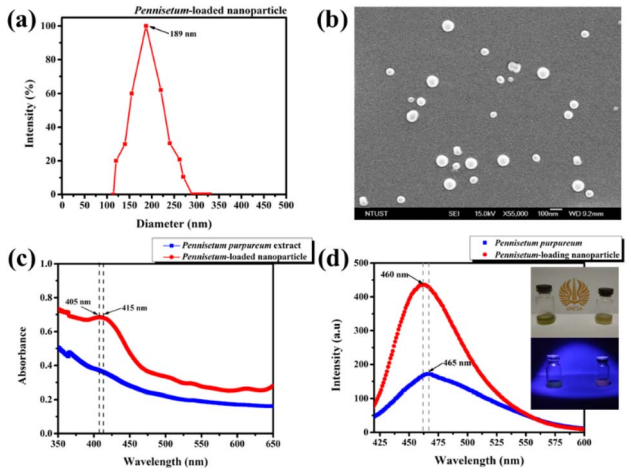

Fig. 1 (a) DLS of *Pennisetum purpureum*-loaded supramolecular nanoparticles. (b) Morphology of *Pennisetum purpureum*-loaded supramolecular nanoparticles by SEM. Optical properties of *Pennisetum purpureum*-loaded supramolecular nanoparticles (c) UV-Vis spectra, and (d) PL spectra.

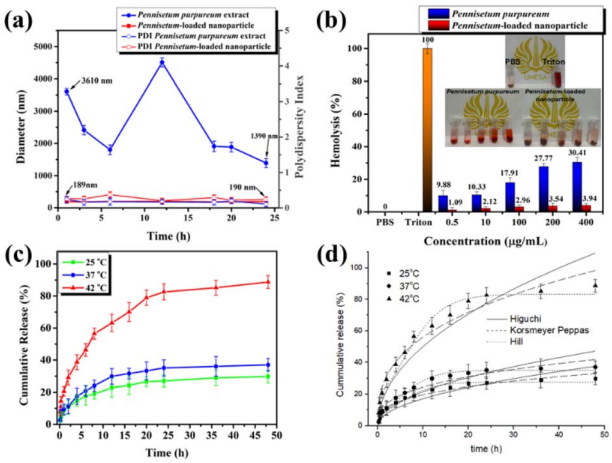

Fig. 2 (a) Kinetic stability of *Pennisetum purpureum* extract and *Pennisetum purpureum*-loaded supramolecular nanoparticles under serum-rich medium. (b) *In vitro* antihemolytic study of *Pennisetum purpureum* extract and *Pennisetum purpureum*-loaded supramolecular nanoparticles (inset figure: photograph of antihemolytic assays). *In vitro* drug release of *Pennisetum purpureum*-loaded supramolecular nanoparticles under different temperatures (c). Kinetic modeling of drug release of *Pennisetum purpureum*-loaded supramolecular nanoparticles (d).

nanoparticles exhibited extensive optical absorbance and a slightly red-shifted peak (415 nm), likely due to conformational changes of *Pennisetum purpureum* within the polymer matrix.[57] Notably, absorption of *Pennisetum purpureum*-loaded nanoparticles significantly exceeds that of *Pennisetum purpureum* extract, indicating more absorption capacity for light intensity absorption relative to the *Pennisetum purpureum* extract. Furthermore, charge carrier dynamics were examined by the measurement of emission spectra using PL. *Pennisetum purpureum*-loaded nanoparticles had distinct emission peaks around 460 nm, which were somewhat blue-shifted and exhibited a high intensity of about 500 a.u, compared to *Pennisetum purpureum* extract, which had intensity only 150 a.u emission peaks at 465 nm (Fig. 1d). These significant findings suggest that the *Pennisetum purpureum* extract within the supramolecular structures has distinctive fluorescence activity, which may be utilized in bioimaging to regulate the distribution of *Pennisetumpurpureum*.[59]

Next, the requisite nanocarrier must exhibit stability within the physiological milieu to be assessed as a potentially viable delivery system utilizing serum-rich medium and mouse red blood cells (MRBCs).[60,61] As shown in Fig. 2a, the hydrodynamic diameter of *Pennisetum purpureum*-loaded nanoparticles remains relatively constant after 24 h, suggesting that host–guest interactions inside the nanoparticles are crucial for preserving structural stability in aqueous solution, while *Pennisetum purpureum* extract exhibited a notable alteration in particle size, decreasing from 3610 nm to 1390 nm. This change was due to the instability of *Pennisetum purpureum* extract particles in the dispersion medium; hydrophobic components within *Pennisetum purpureum* extract tend to reduce particle-solvent affinity when dispersed in medium, leading to aggregation and an increase in hydrodynamic diameter over time. In addition, the pristine supramolecular nanoparticles exhibited a similar tendency to *Pennisetum purpureum*-loaded nanoparticles, which maintained a constant hydrodynamic diameter after 24 h (Fig. S3). Furthermore, drug delivery nanoparticles must maintain a haemolysis rate below 5% (ASTM F756-17 standards) are considered non-haemolytic and biocompatible. Consistent with the stability results in rich-serum medium, an initial antihemolytic investigation with Mouse Red Blood Cells (MRBCs) demonstrated that *Pennisetum purpureum* extract exhibited a haemolysis rate of 30.41% at the highest tested concentration (400 μg mL^{-1}), indicating that *Pennisetum purpureum* extract may exceed the safety limit and suggests potential membrane disruption or toxicity in direct blood contact. Interestingly, *Pennisetum purpureum*-loaded nanoparticles exhibited no hemolytic action at concentrations beyond 400 μg mL^{-1}, remaining well within the non-toxic range below the 5% threshold.[62–64] This finding suggests that nanoparticle encapsulation significantly enhances the hemocompatibility of the extract, potentially mitigating its direct cytotoxic effects upon release (Fig. 2b). Overall, *Pennisetum purpureum*-loaded nanoparticles exhibit structural stability in serum-rich solutions and demonstrate compatibility with MRBCs, indicating their potential promise as a safe and effective drug delivery system, thereby supporting their suitability for *in vivo* applications.

To understand the controlled drug release of *Pennisetum purpureum*-loaded nanoparticles in potentially destroying foam cells in vascular, we investigated the *in vitro* release behavior of *Pennisetum purpureum* from nanoparticles using the dialysis diffusion method at different temperatures (25 °C, 37 °C, and 42 °C) in an inflammatory mimicking environment.[11,12] As indicated in Fig. 2c, cumulative release studies demonstrated *Pennisetum purpureum*-loaded nanoparticles had sustained drug release at temperatures of 25 °C and 37 °C, with 29% and 36%

of *Pennisetum purpureum* released after 48 h, respectively. Under physiological body temperature (37 °C), the polymer chains remain in a semi-rigid state, limiting molecular mobility and thereby retarding the release rate. This controlled release behaviour is desirable for therapeutic applications, as it prevents rapid release and allows for prolonged bioavailability of *Pennisetum purpureum* extract. More importantly, *Pennisetum purpureum*-loaded nanoparticles exhibited a markedly accelerated release of *Pennisetum purpureum* at 42 °C. Over 80% of the *Pennisetum purpureum* was liberated from nanoparticles within the first 24 h, followed by a gradual, continuous release that reached 88% after 48 h. These findings indicate that *Pennisetum purpureum*-loaded nanoparticles exhibit a thermosresponsive release behavior, attributed to a thermally induced hydrophilic–hydrophobic phase transition at 40 °C, which aligns with our previous study on drug release.[48] Thus, *Pennisetum purpureum*-loaded nanoparticles serve as a smart control material for a drug delivery system. These promising results prompted further investigation into the control of drug release through kinetic modeling. The experimental drug release of *Pennisetum purpureum*-loaded nanoparticles exhibited a temperature-responsive behaviour, with the cumulative release increasing as the temperature rose, in the sequence 42 °C > 37 °C > 25 °C, as observed in Fig. 2d. Several drug release models were used to further understand the mechanism of drug release profile against the effect of temperature. It was observed that Higuchi could fit rather well at the initial condition (up to 1 h), but the overall fitting data is not satisfactory. The Korsmeyer Peppas model has more flexibility than the Higuchi model, which confirms the Fickian diffusion behaviour since the value of n is less than 0.5, especially at 42 °C. The fitting of Korsmeyer Peppas has a better fit than Higuchi. The sustained release profile of *Pennisetum purpureum* extract could be fitted well with the Hill equation, in which the parameter of R_m also predicts the maximum cumulative release stated in Table S2. The drug release mechanism of *Pennisetum purpureum*-loaded nanoparticles in solution is based on pore relaxation and swelling. Overall, these finding proves that potential *Pennisetum purpureum*-loaded nanoparticles possess a smart well-controlled drug release within an inflammatory environment, thereby enhancing the precision and effectiveness of targeted therapy.

Atherosclerosis is characterized as a chronic inflammatory disorder, with foam cell formation playing a critical role in its pathogenesis.[65,66] Hence, macrophages treated with oxidized low-density lipoprotein (oxLDL), which simulates foam cell formation, were employed as an *in vitro* model to assess the therapeutic potential of *Pennisetum purpureum*-loaded supramolecular nanoparticles. We first assessed the safety of blank supramolecular nanoparticles towards RAW264.7 cells, and minimal cytotoxicity was detected in RAW264.7 cells, even at a concentration of 500 μg mL^{-1} of supramolecular nanoparticles, indicating that the polymeric carrier of the nanoparticles likely formed a hydrophilic surface layer, which minimized nonspecific membrane adsorption and oxidative stress, thereby maintaining cellular integrity and viability (Fig. 3a). Moreover, foam cells were generated by treating the murine macrophage cell line RAW 264.7 with oxLDL at

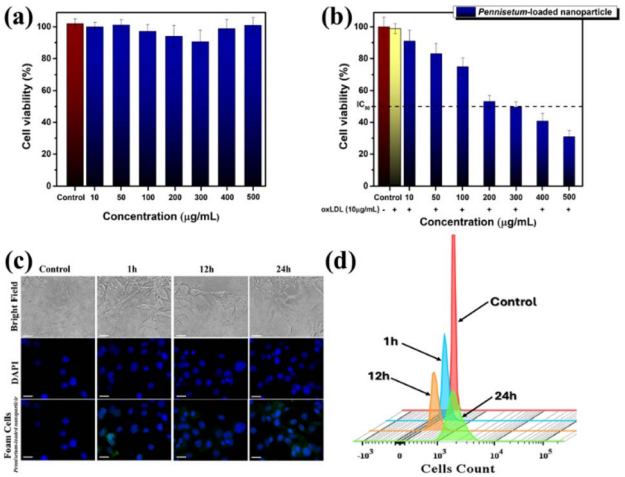

Fig. 3 (a) The viability of RAW264.7 cells treated with supramolecular nanoparticles. (b) The viability of RAW264.7 cells induced by oxLDL (10 μg mL^{-1}) and concurrently treated with *Pennisetum purpureum*-loaded supramolecular nanoparticles. (c) Cellular uptake by CLSM of *Pennisetum purpureum*-loaded supramolecular nanoparticles toward RAW264.7 cells treated with oxLDL. Scale bar: 30 μm. (d) Intracellular analysis by flow cytometry of *Pennisetum purpureum*-loaded supramolecular nanoparticles toward RAW264.7 cells treated with oxLDL. The white scale bars in all CLSM images represent a length of 10 μm.

a concentration of 10 μg mL^{-1} for 24 h. These cells are highly stable and responsive to oxLDL; upon exposure to oxLDL, they take up lipids in an unregulated manner, accumulating cholesterol esters and forming foam cells.[67,68] As depicted in Fig. 3b, co-treatment of macrophages with *Pennisetum purpureum*-loaded nanoparticles had a marked cytotoxic impact with IC_{50} = 310 μg mL^{-1}; yet cell viability improved in a dose-dependent manner. These results suggest that the structural integrity of the *Pennisetum purpureum*-loaded nanoparticles was significantly compromised in the foam cell formation environment induced by oxLDL, which is attributable to the elevated temperature and inflammatory conditions characteristic of such an environment, which facilitated the release of the encapsulated bioactive compounds of *Pennisetum purpureum* extract and subsequently triggered the intended pharmacological effect. Notably, *Pennisetum purpureum*-loaded nanoparticles demonstrated the ability to selectively target inflammatory environments, primarily due to the presence of folic acid (FA) within a supramolecular polymer that has a high affinity for folate receptors, which are overexpressed on activated macrophages within atherosclerotic plaques.[65,66] In addition, this targeting mechanism not only facilitates site-specific drug delivery but may also contribute to the attenuation and delayed progression of atherosclerotic lesions.[14]

The current drug delivery systems are often intercepted by the mononuclear phagocyte system before reaching their intended location.[69,70] This study assessed the absorption efficiency of *Pennisetum purpureum*-loaded nanoparticles by macrophages to elucidate the underlying mechanisms of cellular internalization and intracellular drug release. The nuclei were labeled with blue fluorescence DAPI, whereas the

Pennisetum purpureum-loaded nanoparticles displayed high green fluorescence emissions. As illustrated in Fig. 3c, negligible green fluorescence was detected in control macrophages treated with *Pennisetum purpureum*-loaded nanoparticles, indicating that the drug delivery system enveloped in a macrophage membrane may provide an effective strategy to evade macrophage-mediated clearance. Interestingly, upon treatment of macrophages with oxLDL to promote foam cell formation, a pronounced green fluorescence was observed diffusely within the cytoplasm after 1 h of incubation with *Pennisetum purpureum*-loaded nanoparticles and the green fluorescence signal progressively relocated to the nucleus after 24 h of incubation, suggesting that *Pennisetum purpureum*-loaded nanoparticles have significantly enhanced uptake efficiency in macrophages induced to form foam cells. To validate the CLSM data, quantitative flow cytometry analysis was performed to further investigate the cellular uptake of *Pennisetum purpureum*-loaded nanoparticles by macrophages differentiated into foam cells. As shown in Fig. 3d, the fluorescence intensity significantly increased to strong fluorescence toward macrophages differentiated into foam cells after 24 h of incubation with *Pennisetum purpureum*-loaded nanoparticles, indicating that the supramolecular nanoparticles exhibit a strong affinity for foam cell-differentiated macrophages, thereby promoting rapid internalization of the nanoparticles and ultimately reducing foam cell formation. Overall, these findings demonstrate that *Pennisetum purpureum*-loaded nanoparticles have the potential to modulate oxLDL-induced foam cell formation from macrophages *in vitro*, indicating their considerable potential as smart biomaterials for atherosclerosis therapy.

Molecular docking analysis was conducted to evaluate the interactions between the protein that has contributed to plaque formation and β-CD supramolecular nanoparticles (CD-Sn). Lp-PLA2 was chosen as a protein target in this study because Lp-PLA2 is an enzyme found in the bloodstream and within atherosclerotic plaques. It is involved in the inflammatory processes that contribute to plaque development and rupture.[71,72] Thus, Lp-PLA2 is a promising target for molecular docking studies, particularly in terms of cardiovascular disease and related conditions such as atherosclerosis. Molecular docking analysis revealed that the CD-Sn could bind with Lp-PLA2, although the binding energy was not lower than that of the native ligand, indicating slightly weaker predicted binding strength. However, the CD-Sn formed hydrogen bonds and hydrophobic interactions with amino acid residues compared with native ligand binding (Fig. 4). The interaction between CD-Sn and Lp-PLA2 revealed that CD-Sn can act as a drug delivery vehicle for *Pennisetum purpureum* to the protein target, rather than simply acting as an inhibitor.

To further investigate the dynamic stability and binding behaviour of Lp-PLA$_2$ in complex with CD-Sn and the native ligand, a 100-nanosecond molecular dynamics (MD) simulation was conducted. The analysis focused on protein backbone stability (RMSD), ligand mobility, and residue flexibility (RMSF). The RMSD analysis of the protein backbone indicated that both ligand-bound systems achieved equilibrium after approximately 10–15 ns. The Lp-PLA$_2$ complex with the native

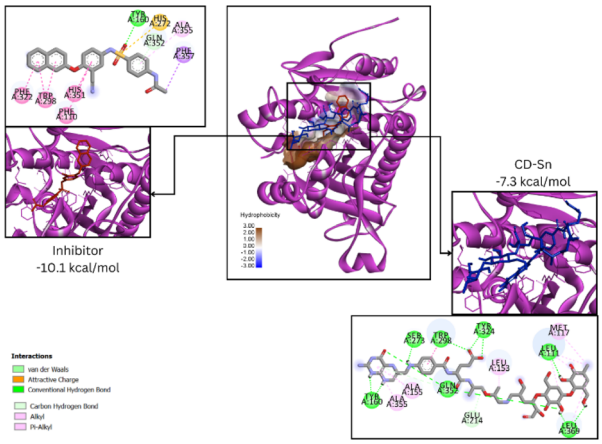

Fig. 4 Visualization of molecular docking result between Lp-PLA2 protein and the ligand; left: native ligand; right: nanoparticles molecule.

ligand exhibited slightly lower overall RMSD values, averaging around 1.6 Å throughout the simulation. In comparison, the CD-Sn complex exhibited marginally higher RMSD values, ranging from 1.8 to 2.0 Å, with no significant structural deviation observed (Fig. 5a). The results suggest that both complexes maintained structural stability during the simulation, with no major conformational rearrangements of the protein backbone. Ligand RMSD analysis revealed a marked difference in the mobility of the two ligands. The native ligand exhibited greater fluctuations, with RMSD values averaging 6.5–7.5 Å and reaching up to 9–10 Å at several time points. This behaviour indicates a higher degree of mobility and possibly weaker interaction with the active site of Lp-PLA$_2$. In contrast, CD-Sn showed more restrained movement, with RMSD values stabilizing around 4.0–5.5 Å, indicating that the ligand maintained a relatively stable conformation within the binding pocket (Fig. 5b). The reduced fluctuation of CD-Sn implies a potentially stronger and more consistent interaction with the protein. Large fluctuations demonstrate that the molecules undergo significant structural changes, while smaller fluctuations indicate a more stable or rigid structure.[71–74] The RMSF analysis of Cα atoms was performed to evaluate the flexibility of amino acid residues during the simulation. Both complexes demonstrated similar fluctuation patterns, with most residues showing RMSF values below 2.0 Å. Notably, higher fluctuations were observed at residues ACE92, LEU93, and GLN427 in both systems, corresponding to flexible loop or terminal regions, which is a common observation in protein dynamics. Importantly, the Lp-PLA$_2$–CD-Sn complex consistently exhibited slightly reduced RMSF values across several residues compared to the native ligand complex, suggesting enhanced local stability upon CD-Sn binding (Fig. 5c). Collectively, the molecular dynamics data indicate that CD-Sn forms a more stable interaction with Lp-PLA$_2$ compared to the native ligand. This is evidenced by the reduced ligand mobility, comparable protein backbone stability, and lower fluctuations in residue positions. These findings suggest that CD-Sn may serve as a promising candidate for Lp-PLA$_2$

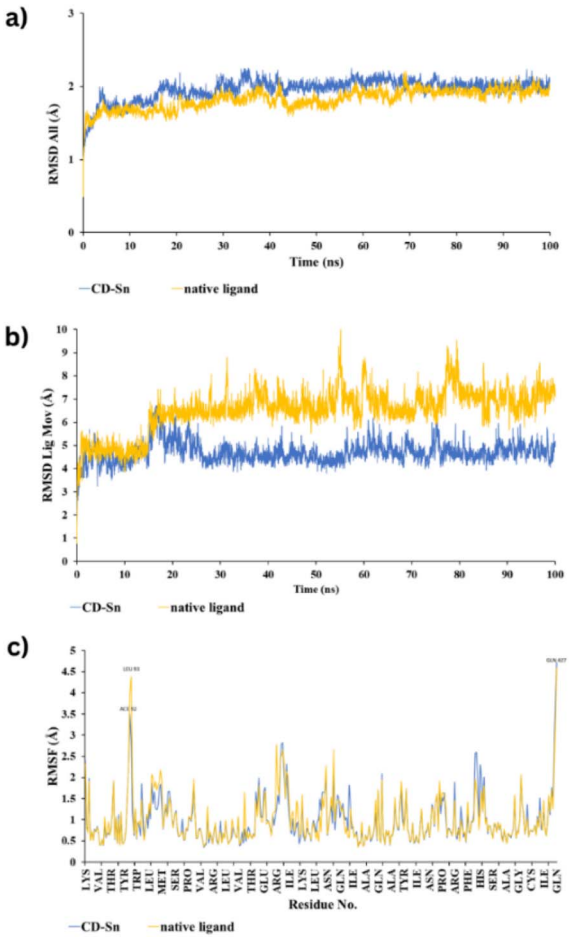

Fig. 5 Molecular dynamics simulation of the Lp-PLA2 complex over 100 ns simulation. (a) RMSD ligand-complex, (b) RMSD ligand movement, (c) root mean square fluctuation (RMSF).

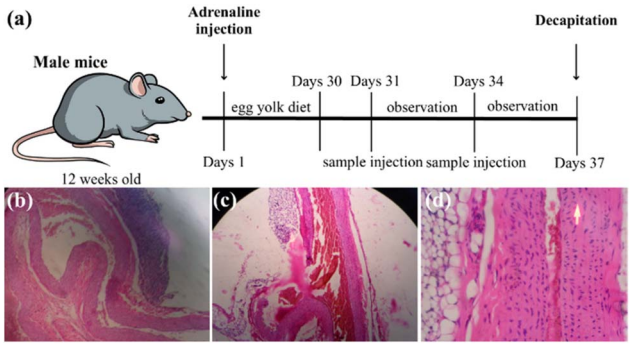

Fig. 6 (a) Schematic illustration of the development of a foam cell mice model induced by adrenaline administration and an egg yolk-enriched diet, followed by treatment with *Pennisetum purpureum* extract and *Pennisetum purpureum*-loaded nanoparticles. The thickness of abdominals aorta with HE staining using 400× magnifications (b) G1, (c) G2, and (d) G3.

inhibition, warranting further investigation through experimental validation and binding free energy analysis.[75]

To evaluate the therapeutic efficacy of *Pennisetum purpureum* extract and *Pennisetum purpureum*-loaded nanoparticles that can destroy foam cells and act as antioxidants in atherosclerotic development, we applied *in vivo* studies divided into 3 groups ($n = 6$ in each group) as G1: control, G2: *Pennisetum purpureum* extract and G3: *Pennisetum purpureum*-loaded nanoparticles. Then, the mice were induced by adrenaline and an egg yolk-enriched diet to create an atherogenic model characterized by thickening of the abdominal aortic wall, followed by treatment with the samples. The abdominal aortic wall was then observed under microscopy after being stained with haematoxylin and eosin (HE) (Fig. 6a).[76–78] Based on Table S3, statistical analysis reveals that G1 has the highest mean and median values of abdominal aorta thickness, which were 68.55 and 69.58, respectively. Meanwhile, G3 has the thinnest abdominal aorta, with a mean value of 61.91 and a median of 60.91, respectively. Interestingly, observation under microscopy with HE also confirmed that G2 and G3 have thickness abdominal aortic thinner with present characteristic slightly rough endothelial surface, protrusion of the tunica intima, and no signs of inflammation compared with G1 displayed that slippery endothelial surface, there no protrusion of the tunica intima, and signed of inflammation with blue colour under HE staining, suggesting that *Pennisetum purpureum*-loaded nanoparticles significantly reduces foam cells on atherogenic diet due to the present bioactive compounds as saponin and FA within nanoparticles (Fig. 6b–d). The aforementioned data clearly indicate that *Pennisetum purpureum*-loaded nanoparticles have the potential to reduce foam cell formation in mice by regulating blood lipid profiles and exerting anti-inflammatory effects.

To further assess the significance of differences among the treatment groups, a One-Way ANOVA was performed. As shown in Table S5, one-way Anova results were obtained with a p-value $= 0.041 < \alpha = 0.05$, indicating that there are differences between G1 and treatments (G2 and G3) with *Pennisetum purpureum* extract and *Pennisetum purpureum*-loaded nanoparticles. Moreover, to understand the significant differences between *Pennisetum purpureum* extract and *Pennisetum purpureum*-loaded nanoparticles in each group, we analysed them using *post hoc* Tukey-HSD. As shown in Table S6, there is significant difference appear between G1 and G3 with p-value $= 0.039 < \alpha = 0.05$, whereas there is no difference between G1 and G2 with p-value $= 0.648 > \alpha = 0.05$. The results suggest that *Pennisetum purpureum*-loaded nanoparticles may be effective in reducing foam cells induced by an atherogenic diet. The accumulated evidence suggests that *Pennisetum purpureum*-loaded nanoparticles exhibit superior therapeutic efficacy against atherosclerosis in mice, potentially outperforming the extract alone. Thus, the encapsulation of natural bioactive compounds into FA-PPG-β-CD supramolecular nanoparticles significantly enhances targeted delivery, effectively mitigating inflammation and foam cell proliferation in an atherogenic model, thereby improving the therapeutic efficacy against atherosclerosis.

Moreover, *in vivo* haematology, liver, and kidney function data were obtained to understand the toxicity effect on other organs. As shown in Table 1, the animals treated with *Pennisetum purpureum*-loaded nanoparticles maintained normal leukocyte, basophil, eosinophil, and lymphocyte levels (28.46 ×

Table 1 *In vivo* blood test of male mice

Category	Test	G1	G2	G3	Normal
Haematology	Haemoglobin	17.7	16.9	16.3	16.5–21.5 g dL^{-1}
	Erythrocytes	6.15	5.48	5.52	4.10–6.10 × 10^6 μL^{-1}
	Haematocrit	50.1	56.5	53.4	48.0–68.0%
	Leukocytes	82.89	35.21	28.46	9.00–37.00 × 10^3 μL^{-1}
	Eosinophils	8.3	3.7	4.1	1.0–5.0%
	Basophil	13.5	0.8	0.5	0.0–1.0%
	Neutrophils	0.6	2.7	1.7	17.0–68.0%
	Lymphocytes	83.2	74.9	68.8	20.0–70.0%
	Platelets	359	230	377	150–450 × 10^3 μL^{-1}
Liver function	Albumin	2.5	3.3	3.1	3.4–4.8 g dL^{-1}
	Globulin	3.2	2.3	2.4	2–3.5 g dL^{-1}
	Total protein	4.9	5.9	5.4	6.0–8.0 g dL^{-1}
	SGOT	224	135	34	0–35 U L^{-1}
	SGPT	50	41	34	0–35 U L^{-1}
Kidney function	BUN	43.5	37.5	17.5	8–18 mg dL^{-1}
	Urea	34	25	29	17–43 mg dL^{-1}
	Creatinine	5.40	3.11	0.19	0.6–1.1 mg dL^{-1}

10^3 μL^{-1}, 0.5%, 4.1%, 68%, respectively), while exhibiting elevated inflammatory markers compared to the untreated atherogenic control group (82.89 × 10^3 μL^{-1}, 13.5%, 8.3%, 83.2%, respectively). Furthermore, liver and kidney function parameters remained within normal ranges on SGOT, SGPT, BUN and creatinine (34 U L^{-1}, 34 U L^{-1}, 17.5 mg dL^{-1}, 0.19 mg mL^{-1}, respectively) after nanoparticle treatment. This contrasts with only *Pennisetum purpureum* extract group, which exhibited elevated liver and kidney function parameters, suggesting organ stress likely due to poor extract stability. Although these findings indicate good biocompatibility of the nanoparticle formulation, further studies on nanoparticle physicochemical stability, tissue biodistribution, and long-term toxicity are required and will be addressed in future research.

Conclusion

In this study, we successfully developed smart controlled release of supramolecular nanoparticles through host–guest interactions involving β-cyclodextrin (β-CD), polypropylene glycol (PPG), and folic acid (FA) creating FA-PPG-β-CD supramolecular nanoparticles that accommodated bioactive compounds of *Pennisetum purpureum* extract, effectively reducing the growth of foam cells in atherosclerotic plaques. *Pennisetum purpureum*-embedded nanoparticles could spontaneously self-assemble into a nanostructure due to the presence of host–guest interaction with unique properties, including green fluorescence, highly stable nanostructure under a serum-rich environment and great biocompatibility with low haemolytic activity. More importantly, *Pennisetum purpureum*-embedded nanoparticles exhibit well-controlled drug release through thermos-responsive properties, as demonstrated in both experimental conditions and kinetic modelling. Furthermore, *in vitro* analysis of RAW 264.7 cells treated with oxLDL at a concentration of 10 μg mL^{-1} clearly demonstrated that *Pennisetum purpureum*-loaded nanoparticles reduced foam cell formation due to the elevated temperature surrounding of inflammatory condition and specific target owing to the presence of folic acid (FA) within the supramolecular have a high affinity for folate receptors. Interestingly, molecular docking analysis revealed that the supramolecular nanoparticles exhibit a specific binding affinity for the Lp-PLA_2 protein, characterized by highly stable interactions associated with cardiovascular diseases, particularly atherosclerosis. Notably, *in vivo* studies have demonstrated that *Pennisetum purpureum*-loaded nanoparticles rapidly destroy excess foam cells in the atherosclerotic aorta, characterized by a slightly rough endothelial surface and protrusion of the tunica intima. In addition, *in vivo* haematology, liver, and kidney function remained within normal ranges when treated with *Pennisetum purpureum*-loaded nanoparticles, indicating good biocompatibility and the absence of toxic effects on other organs. Taken together, this study highlights the encapsulation of bioactive compounds from *Pennisetum purpureum* extract into supramolecular nanoparticles as an effective strategy for reducing foam cells in atherosclerotic plaque and enhancing the therapeutic potential of natural bioactive compounds. Therefore, a more comprehensive assessment including plaque area quantification, macrophage infiltration, and oxidative markers will be addressed in future work.

Experimental section

Materials and chemicals

All chemical reagents were procured from Sigma-Aldrich (St. Louis, MO, USA) and were of the highest available purity. All solvents used were of high-performance liquid chromatography (HPLC) grade and were obtained from TEDIA (Fairfield, OH, USA). FA-PPG-β-CD supramolecular nanoparticles were synthesized and characterized based on the methodology described in our previous report.[51] *Pennisetum purpureum* was obtained from Madura, East Java, Indonesia was processed to obtain leaf extracts as described in our previous study.[48]

Pennisetum purpureum-loaded supramolecular nanoparticles

Briefly, supramolecular nanoparticles at a concentration of 3 mg mL^{-1} were dispersed in an aqueous solution and subjected to continuous stirring and heating, inducing a phase transition from a hydrophilic to a hydrophobic state. Subsequently, different amounts of *Pennisetum purpureum* extract (ranging from 1.0 to 1.5 mg) were gradually added to the solution. The purification of unloaded *Pennisetum purpureum* extract was performed by centrifugation at 6000 rpm for 10 min, then the supernatant was collected as *Pennisetum purpureum*-loaded supramolecular nanoparticles. The loading extract of *Pennisetum purpureum* into the supramolecular nanoparticles was determined using a Genesys-30 UV-Vis spectrophotometer at a wavelength of 405 nm as standard calibration curve prepared from *Pennisetum purpureum* leaf extract in ethanol. Drug loading efficiency (DLE) and drug loading content (DLC) were calculated using the following formulas:

$$\mathrm{DLC}(\%) = \frac{\text{Weight of drug loaded in nanoparticle}}{\text{Weight of drug loaded nanoparticle}} \times 100$$

$$\mathrm{DLE}(\%) = \frac{\text{Weight of drug loaded in nanoparticle}}{\text{Weight of drug input}} \times 100$$

Determination of dynamic hydrodynamic diameter and zeta potential

The hydrodynamic particle size and charge stability of the samples were determined using a dynamic light scattering (DLS) particle analyser (Nano Brook 90Plus PALS, Brookhaven, USA) equipped with a 632 nm He–Ne laser source and a fixed scattering angle of 90°. Each sample was measured in triplicate, and the results were averaged to obtain a representative value.

Ultraviolet-visible (UV-vis) and photoluminescence (PL). Optical properties were analysed by Genesys-30 UV-Vis spectrophotometer within the wavelength range of 350 to 650 nm and Shimadzu RF-5301 (Hitachi, Tokyo, Japan) using an excitation wavelength of 415 nm and a scanning range from 425 to 600 nm.

Scanning electron microscopy (SEM). Field-emission scanning electron microscopy (FE-SEM; JSM-6500, JEOL, Tokyo, Japan) was conducted to observe the morphology of pristine supramolecular nanoparticles, *Pennisetum purpureum* leaf extract, and *Pennisetum purpureum*-loaded nanoparticles.

Analysis of the dynamic stability profile

The stability of pristine *Pennisetum purpureum* leaf extract and *Pennisetum purpureum*-loaded nanoparticles in DMEM media was evaluated in the presence of fetal bovine serum (FBS), which served as a destabilizing agent. Pristine *Pennisetum purpureum* leaf extract, and *Pennisetum purpureum*-loaded nanoparticles were mixed with DMEM supplemented with serum. The dispersion stability was evaluated by monitoring the light scattering intensity using DLS over a 24 h period.

Antihemolytic analysis

Mouse red blood cells (MRBCs) were employed to evaluate the antihemolytic activity of pristine *Pennisetum purpureum* leaf extract and *Pennisetum purpureum*-loaded nanoparticles, following the procedure described in a previously established method.[52]

Time-dependent drug release profile of *Pennisetum purpureum*-loaded nanoparticles

To generate the drug release profiles, dialysis tubing with a molecular weight cut-off (MWCO) of 1000 Da was filled with *Pennisetum purpureum*-loaded nanoparticles and immersed in phosphate-buffered saline (PBS, pH 7.4). The samples were subjected to moderate agitation and incubated for 48 h at varying temperatures (25 °C, 37 °C, and 42 °C). At predetermined time intervals (0.25, 0.5, 1, 2, 4, 6, 8, 12, 16, 20, 24, 36, and 48 h), 5 mL of the dialysis buffer was withdrawn and immediately replaced with an equal volume of fresh PBS to maintain sink conditions. The amount of *Pennisetum purpureum* released was quantified using UV-Vis spectroscopy by measuring the absorbance of the samples and comparing the values to a standard calibration curve. The release profile of *Pennisetum purpureum* from the nanoparticles was determined by plotting the cumulative amount of *Pennisetum purpureum* released over time, based on the following equation:

$$\text{Cumulative drug release}(\%) = \frac{W_t}{W} \times 100$$

In this equation, W_t represents the amount of *Pennisetum purpureum* released at a given time t, while W denotes the total amount of *Pennisetum purpureum* encapsulated within the nanoparticles. The results were obtained from three independent experiments, each performed in triplicate, and are expressed as the mean ± standard deviation (SD).

Simulation of drug release

The drug release profile was evaluated by monitoring the cumulative percentage of drug released over time. The *in vitro* release data were plotted and fitted into three different kinetic models to understand the release mechanism and to identify the best-fitting model describing the release behaviour from the drug delivery system. The release profiles were analysed using the following models:

$$R_t = \frac{R_\mathrm{m}\, t^a}{\left(t_{1/2} + t^a\right)} \quad \text{(a)}$$

$$R_t = k_\mathrm{P} t^n \quad \text{(b)}$$

$$R_t = k_\mathrm{H} t^{0.5} \quad \text{(c)}$$

Eqn (a)–(c) represent the model fitting of Sigmoidal Hill, Korsmeyer–Peppas, and Higuchi, respectively. Where R_t is the cumulative release of the drug at a certain time (%), t is the time (h), R_m is the maximum release of the drug (%), $t_{1/2}$ is the time to reach half of the maximum cumulative release (h), a is

defined as a characteristic sigmoidal factor that is specific for a certain drug and carrier system, k_P is the Korsmeyer–Peppas constant, n is the release exponent, and k_H is the Higuchi constant.

Cell culture

The Stem Cell Research and Development Centre, Universitas Airlangga, Surabaya, Indonesia, provided the RAW 264.7 cell line. RAW 264.7 cells were cultured in a humidified incubator at 37 °C with 5% CO_2, using high-glucose DMEM supplemented with 10% FBS and 1% penicillin-streptomycin. Prior to each experiment, cells were detached using trypsin–EDTA and subsequently resuspended in PBS containing 0.1% trypan blue for viability assessment and cell counting using a hemacytometer.

Cell-based safety evaluation of *Pennisetum purpureum*-loaded nanoparticles

Cytotoxic effects of pristine nanoparticles were evaluated *in vitro* using the MTT assay conducted on RAW 264.7 macrophage cells. Briefly, cells were seeded into 96-well plates at a density of 1×10^6 cells per mL. Following a 24 h incubation, the culture medium was replaced with fresh medium containing pristine nanoparticles at various concentrations (10, 50, 100, 200, 300, 400, and 500 μg mL^{-1}), respectively. Then, the medium was replaced with DMEM containing MTT reagent, and cell viability was subsequently determined based on the MTT assay. Absorbance readings were obtained at a wavelength of 570 nm using a microplate reader equipped for ELISA measurements. The percentage of cell viability at each sample concentration was calculated using the following formula:

$$\text{Percentage cell viability} = \frac{\text{Absorbance of treated cell}}{\text{Absorbance of control cell}} \times 100$$

In vitro modulatory effects of *Pennisetum purpureum*-loaded nanoparticles on inflammatory responses

RAW 264.7 cells were incubated for 24 h with culture medium containing oxidized low-density lipoprotein (oxLDL) for 10 μg mL^{-1}, which induced foam cell formation[50] at different concentrations of *Pennisetum purpureum*-loaded nanoparticles (10, 50, 100, 200, 300, 400, and 500 μg mL^{-1}). Cells treated solely with oxLDL served as the positive control group. Upon completion of the incubation period, the culture medium was replaced with DMEM supplemented with MTT reagent and cell viability was quantitatively assessed through the MTT assay.

Visualization of cellular uptake of *Pennisetum purpureum*-loaded nanoparticles by fluorescence microscopy

Intracellular uptake and intracellular drug release assays were performed in macrophages pre-treated with oxLDL under density of 2×10^4 cells per mL. Then, following cell was seeded for 24 h, the culture medium was replaced with fresh medium containing *Pennisetum purpureum*-loaded nanoparticles (IC_{50}; 295 μg mL^{-1}). The cells were then incubated for additional time intervals of 1, 12, and 24 h, respectively. Subsequently, the cells were rinsed three times with PBS and fixed by incubation with 1.5 mL of freshly prepared 4% paraformaldehyde solution for 10 min. The cells were washed three times with PBS and counterstained with DAPI for 15 min. Finally, the cells were subsequently washed with PBS to eliminate any residual stain or fixative and examined using fluorescence microscopy.

Molecular docking

Molecular docking analysis was performed to evaluate the binding affinity of FA-PPG-β-CD supramolecular nanoparticles labelled by (CD-Sn) toward the Lp-PLA2 (PDB ID: 5YE9). The 3D structures of the ligand (nanoparticles) were created using Chem3D 16.0. The ligand control used in this study was the native ligand in Lp-PLA2 (PDB ID: 5YE9). Protein preparation was conducted using Discovery Studio. Docking simulations were carried out using AutoDock Vina equipped with the PyRx 0.8 platform. The grid box was centred on the active site of Lp-PLA2, based on known inhibitor binding regions. Binding affinity scores (in kcal mol^{-1}) were recorded, and ligand–protein interactions were visualized using Discovery Studio Visualizer and BIOVIA. The docking results were compared with known Lp-PLA2 inhibitors. Hydrogen bonding, hydrophobic interactions, and residue involvement in binding were analysed in detail.

Dynamic docking

All selected compounds were subjected to molecular-dynamics (MD) simulations to evaluate the stability and interaction dynamics of the ligand–protein complexes. Simulations were carried out using the Yet Another Scientific Artificial Reality Application (YASARA) software, employing the AMBER14 force field to model atomic interactions. The system was configured to replicate physiological conditions, including a temperature of 310 K (37 °C), pH 7.4, a pressure of 1 atm, and a 0.9% NaCl concentration, to simulate a biologically relevant environment. Each simulation was run for a total duration of 100 nanoseconds (ns), which is sufficient to observe significant conformational changes and assess the stability of the protein–ligand complexes over time. The choice of 310 K aligns with standard human physiological temperature and is widely accepted in molecular dynamics protocols for biomolecular systems.

Formulation of an atherogenic diet and *Pennisetum purpureum*-loaded nanoparticles treatment

Twelve-week-old male mice with approximately body weight 45–55 g, were obtained from a certified experimental animal facility (Ethical Clearance Certificate No. 3.KEH.163.10.2023). Prior to the experiment, the animals were acclimatized to the laboratory environment by being maintained on a standard rodent diet for one week with a temperature of 22–25 °C and under relative humidity of 40–45%. The induction of an atherogenic condition in rats was initiated by intravenous administration of 0.006 mg of adrenaline on the first day, followed by the provision of a high-cholesterol diet to promote hyperlipidemia.[51–53]

Thereafter, the rats received an egg yolk-enriched diet at a dose of 8 mg per of body weight per day for 4 weeks to further elevate serum lipid levels and facilitate the induction of atherosclerotic conditions. The day 31 and 34, *Pennisetum purpureum* extract and *Pennisetum purpureum*-loaded supramolecular nanoparticles with a dose of 1.15 mg per of body weight were injected intravenously with observations conducted throughout this period. On day 37, the subject was sedated with isoflurane (4–5%) and euthanized by decapitation at week six. Then, approximately 5 cm of the abdominal aorta was excised and fixed in 18% paraformaldehyde solution for 18 h, subsequently cut and embedded into 4 μm-thick sections. Finally, for histological analysis, the tissue sections were mounted on poly-L-lysine-coated slides and stained with haematoxylin and eosin (H&E). The stained sections were then examined under a light microscope at 400× magnification.

Statistical analysis

All experiments were conducted in triplicate. Statistical analysis was conducted using one-way ANOVA, followed by Tukey's Honestly Significant Difference (HSD) post hoc test to identify differences between groups. Differences were considered statistically significant at a p-value < 0.05.

Ethical statement

All animal procedures were performed in accordance with the Guidelines for Care and Use of Laboratory Animals of "Universitas Negeri Surabaya" and approved by the Animal Ethics Committee of "Faculty of Veterinary Medicine Airlangga University".

Conflicts of interest

The authors declare no competing financial interest.

Data availability

The authors confirm that the data supporting the findings of this study are available within the article and its supplementary information (SI). Raw data that support the findings of this study are available from the corresponding author, upon reasonable request. Supplementary information: DLS, SEM, kinetic stability, loading content, modelling release, and statistical *in vivo* study results. See DOI: https://doi.org/10.1039/d5ra07519j.

Acknowledgements

This study was supported financially by Direktorat Penelitian dan Pengabdian Kepada Masyarakat (DPPM) (contract no. B/74011/UN38.III.1/LK.04.00/2025).

References

1 A. Roth Gregory, C. Johnson, A. Abajobir, F. Abd-Allah, F. Abera Semaw, G. Abyu, M. Ahmed, B. Aksut, T. Alam, K. Alam, F. Alla, N. Alvis-Guzman, S. Amrock, H. Ansari, J. Ärnlöv, H. Asayesh, M. Atey Tesfay, L. Avila-Burgos, A. Awasthi, A. Banerjee, A. Barac, T. Bärnighausen, L. Barregard, N. Bedi, E. Belay Ketema, D. Bennett, G. Berhe, Z. Bhutta, S. Bitew, J. Carapetis, J. Carrero Juan, C. Malta Deborah, A. Castañeda-Orjuela Carlos, J. Castillo-Rivas, F. Catalá-López, J.-Y. Choi, H. Christensen, M. Cirillo, L. Cooper, M. Criqui, D. Cundiff, A. Damasceno, L. Dandona, R. Dandona, K. Davletov, S. Dharmaratne, P. Dorairaj, M. Dubey, R. Ehrenkranz, M. El Sayed Zaki, A. Faraon Emerito Jose, A. Esteghamati, T. Farid, M. Farvid, V. Feigin, L. Ding Eric, G. Fowkes, T. Gebrehiwot, R. Gillum, A. Gold, P. Gona, R. Gupta, D. Habtewold Tesfa, N. Hafezi-Nejad, T. Hailu, B. Hailu Gessessew, G. Hankey, Y. Hassen Hamid, H. Abate Kalkidan, R. Havmoeller, I. Hay Simon, M. Horino, J. Hotez Peter, K. Jacobsen, S. James, M. Javanbakht, P. Jeemon, D. John, J. Jonas, Y. Kalkonde, C. Karimkhani, A. Kasaeian, Y. Khader, A. Khan, Y.-H. Khang, S. Khera, T. Khoja Abdullah, J. Khubchandani, D. Kim, D. Kolte, S. Kosen, J. Krohn Kristopher, G. A. Kumar, F. Kwan Gene, K. Lal Dharmesh, A. Larsson, S. Linn, A. Lopez, A. Lotufo Paulo, A. El Razek Hassan Magdy, R. Malekzadeh, M. Mazidi, T. Meier, G. Meles Kidanu, G. Mensah, A. Meretoja, H. Mezgebe, T. Miller, E. Mirrakhimov, S. Mohammed, E. Moran Andrew, I. Musa Kamarul, J. Narula, B. Neal, F. Ngalesoni, G. Nguyen, M. Obermeyer Carla, M. Owolabi, G. Patton, J. Pedro, D. Qato, M. Qorbani, K. Rahimi, K. Rai Rajesh, S. Rawaf, A. Ribeiro, S. Safiri, A. Salomon Joshua, I. Santos, M. Santric Milicevic, B. Sartorius, A. Schutte, S. Sepanlou, A. Shaikh Masood, M.-J. Shin, M. Shishehbor, H. Shore, S. Silva Diego Augusto, E. Sobngwi, S. Stranges, S. Swaminathan, R. Tabarés-Seisdedos, N. Tadele Atnafu, F. Tesfay, J. S. Thakur, A. Thrift, R. Topor-Madry, T. Truelsen, S. Tyrovolas, N. Ukwaja Kingsley, O. Uthman, T. Vasankari, V. Vlassov, E. Vollset Stein, T. Wakayo, D. Watkins, R. Weintraub, A. Werdecker, R. Westerman, S. Wiysonge Charles, C. Wolfe, A. Workicho, G. Xu, Y. Yano, P. Yip, N. Yonemoto, M. Younis, C. Yu, T. Vos, M. Naghavi and C. Murray, *JACC*, 2017, **70**, 1–25.

2 O. Gaidai, Y. Cao and S. Loginov, *Curr. Probl. Cardiol.*, 2023, **48**, 101622.

3 P. Zhuang, X. Liu, Y. Li, Y. Ao, Y. Wu, H. Ye, X. Wan, L. Zhang, D. Meng, Y. Tian, X. Yu, F. Zhang, A. Wang, Y. Zhang and J. Jiao, *Nat. Commun.*, 2025, **16**, 437.

4 S. Allahverdian, C. Chaabane, K. Boukais, G. A. Francis and M.-L. Bochaton-Piallat, *Cardiovasc. Res.*, 2018, **114**, 540–550.

5 S. Allahverdian, A. C. Chehroudi, B. M. McManus, T. Abraham and G. A. Francis, *Circulation*, 2014, **129**, 1551–1559.

6 K. J. Moore, F. J. Sheedy and E. A. Fisher, *Nat. Rev. Immunol.*, 2013, **13**, 709–721.

7 I. Tabas and K. E. Bornfeldt, *Circ. Res.*, 2016, **118**, 653–667.

8 M. Bäck, A. Yurdagul, I. Tabas, K. Öörni and P. T. Kovanen, *Nat. Rev. Cardiol.*, 2019, **16**, 389–406.

9 R. Saigusa, H. Winkels and K. Ley, *Nat. Rev. Cardiol.*, 2020, **17**, 387–401.

10 J. Fan and T. Watanabe, *Pathol. Int.*, 2022, **72**, 151–160.
11 C. Stefanadis, L. Diamantopoulos, J. Dernellis, E. Economou, E. Tsiamis, K. Toutouzas, C. Vlachopoulos and P. Toutouzas, *J. Mol. Cell. Cardiol.*, 2000, **32**, 43–52.
12 W. Casscells, W. K. Vaughn, H. McAllister, J. T. Willerson, W. Casscells, J. T. Willerson, W. Casscells, B. Hathorn, M. David, W. Vaughn, H. K. McAllister, J. T. Willerson, T. Krabach and G. Bearman, *Lancet*, 1996, **347**, 1447–1449.
13 S. Bian, Y. Zhu, N. Zhao, Y. Wang, Z. Yang and J. Li, *Mater. Today Bio*, 2025, **32**, 101827.
14 S. Pan, H. Liu, F. Gao, H. Luo, H. Lin, L. Meng, C. Jiang, Y. Guo, J. Chi and H. Guo, *J. Cell. Mol. Med.*, 2018, **22**, 3183–3191.
15 S. Cui, W. Li, X. Lv, P. Wang, G. Huang and Y. Gao, *Appl. Physiol., Nutr., Metab.*, 2017, **42**, 1015–1022.
16 W. Xia, A. R. Hilgenbrink, E. L. Matteson, M. B. Lockwood, J.-X. Cheng and P. S. Low, *Blood*, 2009, **113**, 438–446.
17 R. Carnicer, M. A. Navarro, J. M. Arbonés-Mainar, S. Acín, M. A. Guzmán, J. C. Surra, C. Arnal, M. de las Heras, F. Blanco-Vaca and J. Osada, *Life Sci.*, 2007, **80**, 638–643.
18 R. P. Sijbesma, L. Brunsveld, B. J. B. Folmer, J. H. K. Ky Hirschberg, R. F. M. Lange, J. L. Lowe and E. W. Meijer, *Science*, 1997, **278**(5343), 1601–1604.
19 S.-G. Chen, Y. Yu, X. Zhao, Y. Ma, X.-K. Jiang and Z.-T. Li, *J. Am. Chem. Soc.*, 2011, **133**, 11124–11127.
20 L. Yang, X. Tan, Z. Wang and X. Zhang, *Chem. Rev.*, 2015, **115**, 7196–7239.
21 J. Zhou, G. Yu and F. Huang, *Chem. Soc. Rev.*, 2017, **46**, 7021–7053.
22 J. Zhou, L. Rao, G. Yu, T. R. Cook, X. Chen and F. Huang, *Chem. Soc. Rev.*, 2021, **50**, 2839–2891.
23 H. Tang, W. Zhao, J. Yu, Y. Li and C. Zhao, *Molecules*, 2019, **24**(1), 4.
24 P. Zarrintaj, M. Jouyandeh, M. R. Ganjali, B. S. Hadavand, M. Mozafari, S. S. Sheiko, M. Vatankhah-Varnoosfaderani, T. J. Gutiérrez and M. R. Saeb, *Eur. Polym. J.*, 2019, **117**, 402–423.
25 H. Gu, S. Mu, G. Qiu, X. Liu, L. Zhang, Y. Yuan and D. Astruc, *Coord. Chem. Rev.*, 2018, **364**, 51–85.
26 J. Wang, D. Wang, M. Cen, D. Jing, J. Bei, Y. Huang, J. Zhang, B. Lu, Y. Wang and Y. Yao, *J. Nanobiotechnol.*, 2022, **20**, 33.
27 W. Han, W. Xiang, Q. Li, H. Zhang, Y. Yang, J. Shi, Y. Ji, S. Wang, X. Ji, N. M. Khashab and J. L. Sessler, *Chem. Soc. Rev.*, 2021, **50**, 10025–10043.
28 V. Kumar, T. M. Koyasseril-Yehiya and S. Thayumanavan, in *Molecular Assemblies: Characterization and Applications*, American Chemical Society, 2020, vol. 1355, ch. 7, pp. 95–107.
29 K. Yan, S. Zhang, K. Zhang, Y. Miao, Y. Qiu, P. Zhang, X. Jia and X. Zhao, *Polym. Chem.*, 2020, **11**, 7704–7713.
30 P. Wei, E. J. Cornel and J. Du, *Drug Delivery Transl. Res.*, 2021, **11**, 1323–1339.
31 H. W. Yong and A. Kakkar, *Polym. Int.*, 2022, **71**, 514–520.
32 L. Hu, Q. Zhang, X. Li and M. J. Serpe, *Mater. Horiz.*, 2019, **6**, 1774–1793.
33 L. Wang, L.-L. Li, Y.-S. Fan and H. Wang, *Adv. Mater.*, 2013, **25**, 3888–3898.
34 M. J. Webber, E. A. Appel, E. W. Meijer and R. Langer, *Nat. Mater.*, 2016, **15**, 13–26.
35 A. G. Cheetham, P. Zhang, Y.-a. Lin, L. L. Lock and H. Cui, *J. Am. Chem. Soc.*, 2013, **135**, 2907–2910.
36 G. Yu, K. Jie and F. Huang, *Chem. Rev.*, 2015, **115**, 7240–7303.
37 M. T. Bazana, C. F. Codevilla and C. R. de Menezes, *Curr. Opin. Food Sci.*, 2019, **26**, 47–56.
38 Y. Tang, Q. Cai, Z. Tian, W. Chen and H. Tang, *Research*, 2025, **8**, 0600.
39 M. Xiao, D. Li, Y. Li, Y. Liang, J. Zhang and Z. Song, *Appl. Organomet. Chem.*, 2025, **39**, e70048.
40 Y.-N. Chen, W. M. Kao, S.-C. Lee, J.-M. Wu, Y.-S. Ho and M.-K. Hsieh, *Pathogens*, 2022, **11**(11), 1371.
41 G. E. Mathew, B. Mathew, S. Gokul, R. Krishna and M. P. Farisa, *Ancient Sci. Life*, 2015, **34**(3), 175–178.
42 V. S. Somerville, A. J. Braakhuis and W. G. Hopkins, *Adv. Nutr.*, 2016, **7**, 488–497.
43 C. Huan, W. Xu, B. Ni, T. Guo, H. Pan, L. Jiang, L. Li, J. Yao and S. Gao, *Front. Pharmacol*, 2021, **12**, DOI: 10.3389/fphar.2021.628526.
44 S. H. Nile and S. W. Park, *Nutrition*, 2014, **30**, 134–144.
45 M. Budiyanto, S. Puspitarini, S. Prasetyo, H. Subekti, Y. S. Birhan, A. Qosyim and F. B. Ilhami, *Braz. J. Biol.*, 2024, **84**, e280855.
46 S. Chu, W. Qu, X. Pang, B. Sun and X. Huang, *Zhongyaocai*, 2003, **26**, 341–344.
47 T. Wang, R. C. Y. Choi, J. Li, C. W. C. Bi, W. Ran, X. Chen, T. T. X. Dong, K. Bi and K. W. K. Tsim, *J. Ethnopharmacol.*, 2012, **139**, 214–220.
48 C. Liu, Y.-J. Shen, Q.-B. Tu, Y.-R. Zhao, H. Guo, J. Wang, L. Zhang, H.-W. Shi and Y. Sun, *Biomed. Pharmacother.*, 2018, **101**, 608–616.
49 M. A. Barros-Rodríguez, F. J. Solorio-Sánchez, C. A. Sandoval-Castro, A. M. M. Ahmed, R. Rojas-Herrera, E. G. Briceño-Poot and J. C. Ku-Vera, *Anim. Prod. Sci.*, 2014, **54**, 1486–1489.
50 A. S. Ashour, M. M. A. El Aziz and A. S. Gomha Melad, *J. Nanomed. Res.*, 2019, **7**, 282–288.
51 F. B. Ilhami, E. Erman, A. Rahmawati, Y. S. Birhan, Fitriana and A. H. Tiwikrama, *J. Drug Delivery Sci. Technol.*, 2023, **89**, 105078.
52 J. N. Putro, F. Bintang Ilhami, C.-C. Cheng, K. J. Imanuela, D. Mangindaan, W. Irawaty, A. Rahmawati, O. Shimomura and S. Ismadji, *Int. J. Biol. Macromol.*, 2025, **315**, 144625.
53 L.-H. Shen, L. Zhou, B.-Y. Wang, J. Pu, L.-H. Hu, D.-J. Chai, L. Wang, J.-Z. Zeng and B. He, *Atherosclerosis*, 2008, **199**, 257–264.
54 R. N. Chakravarti, B. Sasi Kumar, C. R. Nair and M. Kumar, *Atherosclerosis*, 1977, **28**, 405–416.
55 H. Winarsi, A. Yuniaty and I. Nuraeni, *Int. Food Res. J.*, 2016, **23**, 2103–2111.
56 E. N. Mohammed, A. M. Soliman and A. S. Mohamed, *J. Food Biochem.*, 2022, **46**, e14296.
57 Q.-D. Hu, G.-P. Tang and P. K. Chu, *Acc. Chem. Res.*, 2014, **47**, 2017–2025.
58 W. Li, W. Xu, S. Zhang, J. Li, J. Zhou, D. Tian, J. Cheng and H. Li, *J. Agric. Food Chem.*, 2022, **70**, 12746–12759.

59 S. Y. Lee, S. I. Jeon, S. B. Sim, Y. Byun and C.-H. Ahn, *Acta Biomater.*, 2021, **131**, 286–301.
60 S. Valdez, M. Robertson and Z. Qiang, *Macromol. Rapid Commun.*, 2022, **43**, 2200421.
61 Y. Ping, D. Ding, R. A. N. S. Ramos, H. Mohanram, K. Deepankumar, J. Gao, G. Tang and A. Miserez, *ACS Nano*, 2017, **11**, 4528–4541.
62 S. H. Jung, D. Bochicchio, G. M. Pavan, M. Takeuchi and K. Sugiyasu, *J. Am. Chem. Soc.*, 2018, **140**, 10570–10577.
63 F. B. Ilhami, S. Puspitarini, Fitriana, A. Rahmawati, N. R. Mayasari and H. Herliniati, *Plant Nano Biol.*, 2025, **11**, 100135.
64 S. Chen, Q. Li, H. Li, L. Yang, J. Z. Yi, M. Xie and L. M. Zhang, *Mater. Sci. Eng., C*, 2020, **109**, 110636.
65 Z. Yu, L. Ma, S. Ye, G. Li and M. Zhang, *Carbohydr. Polym.*, 2020, **236**, 115972.
66 D. J. Rader and E. Puré, *Cell Metab.*, 2005, **1**, 223–230.
67 C. K. Marasinghe, S.-D. Yoon and J.-Y. Je, *BioFactors*, 2024, **50**, 1161–1175.
68 H.-C. Lin, C.-K. Lii, H.-C. Chen, A.-H. Lin, Y.-C. Yang and H.-W. Chen, *Am. J. Chin. Med.*, 2018, **46**, 87–106.
69 J. Fan, L. Liu, Q. Liu, Y. Cui, B. Yao, M. Zhang, Y. Gao, Y. Fu, H. Dai, J. Pan, Y. Qiu, C. H. Liu, F. He, Y. Wang and L. Zhang, *Nat. Commun.*, 2019, **10**, 425.
70 A. L. Moens, C. J. Vrints, M. J. Claeys, J.-P. Timmermans, H. C. Champion and D. A. Kass, *Am. J. Physiol.: Heart Circ. Physiol.*, 2008, **294**, H1971–H1977.
71 A. A. Mangoni, *Clin. Chim. Acta*, 2006, **367**, 11–19.
72 S. Barua and S. Mitragotri, *Nano Today*, 2014, **9**, 223–243.
73 E. Blanco, H. Shen and M. Ferrari, *Nat. Biotechnol.*, 2015, **33**, 941–951.
74 M. Cahyaningtias, M. S. Rohman, Widodo, A. Wahjono Adi, R. Yuda, Y. Indrayana, J. F. Putri, Rusdianto, M. Lukitasari and D. Hendrawan, *Genes Dis.*, 2016, **3**, 289–293.
75 Z. Fras, J. Tršan and M. Banach, *Arch. Med. Sci.*, 2021, **17**, 954–964.
76 Y. Maruyama, R. Igarashi, Y. Ushiku and A. Mitsutake, *J. Chem. Inf. Model.*, 2023, **63**, 1529–1541.
77 H. Winarsi, A. Yuniaty and I. Nuraeni, *Agric. Agric. Sci. Procedia*, 2016, **9**, 264–270.
78 C. A. Che Mohamad, A. B. Abd Fuaat, A. Y. Abdul Wahab, H. A. H. Alfarisi, M. B. Ibrahim and Z. B. H. Mohamed, *ASM Sci. J.*, 2021, **15**, 1–10.